Supporting Information

Engineering Homochiral MOFs in TiO_2 Nanotubes as Enantioselective Photoelectrochemical Electrode for Chiral Recognition

Shanshan Zhou,[†] Junli Guo,[†] Zhenqing Dai,[†] Changyong Liu,[†] Junjian Zhao,[†] Zhida Gao,[†] Yan-Yan Song[†*]

[†]College of Sciences, Northeastern University, Shenyang 110004, China

*E-mail: yysong@mail.neu.edu.cn.

Table of Contents

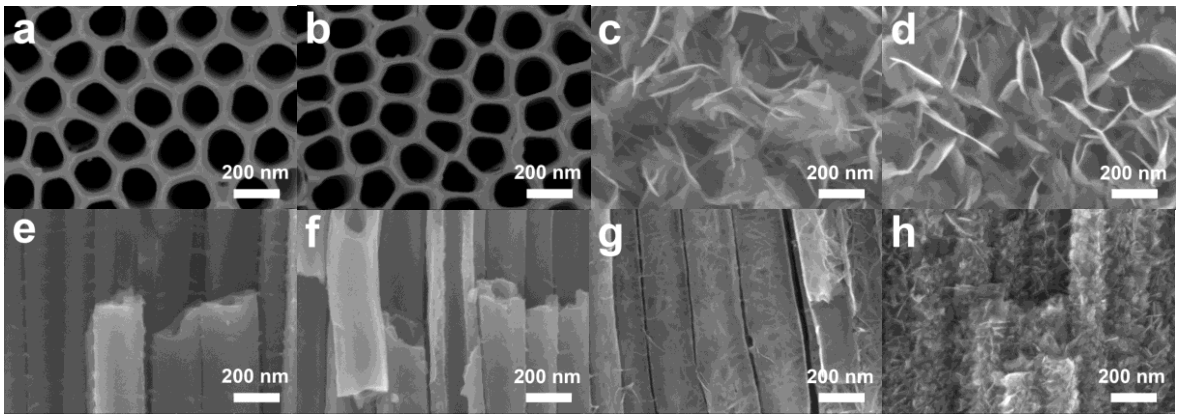

Figure S1. SEM images of (a, e) as-prepared TiO_2 NTs and TiO_2/MIL-125 NTs prepared by adding different amounts of HCl (0.1 M) into BDC-DMF solution for hydrothermal treatment: (b, f) 0 μL, (c, g) 100 μL, and (d, h) 200 μL.

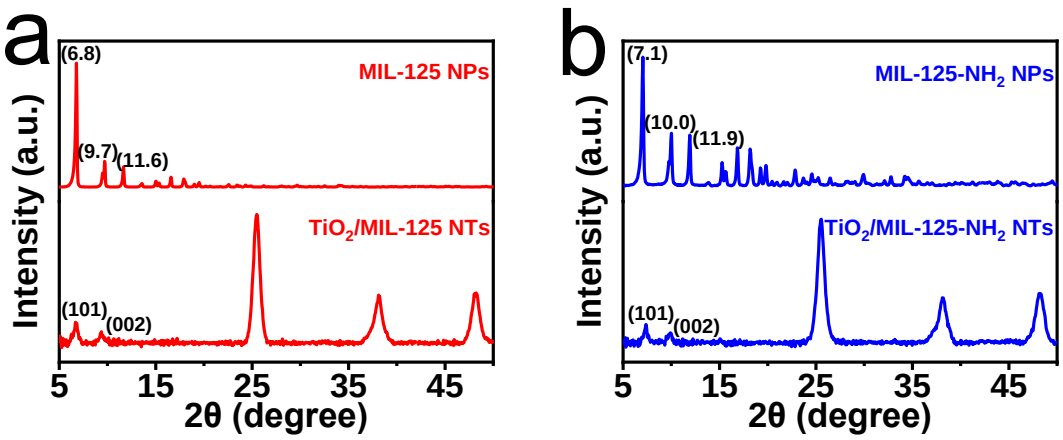

Figure S2. XRD patterns of (a) MIL-125 and TiO_2/MIL-125 NTs, and (b) MIL-125-NH_2 and TiO_2/MIL-125-NH_2 NTs.

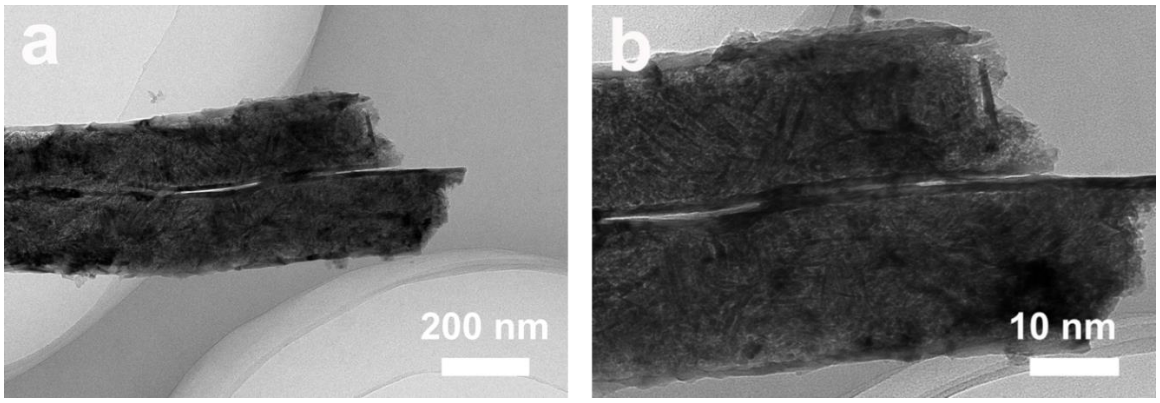

Figure S3. TEM images of TiO_2/MIL-125-NH_2 NTs.

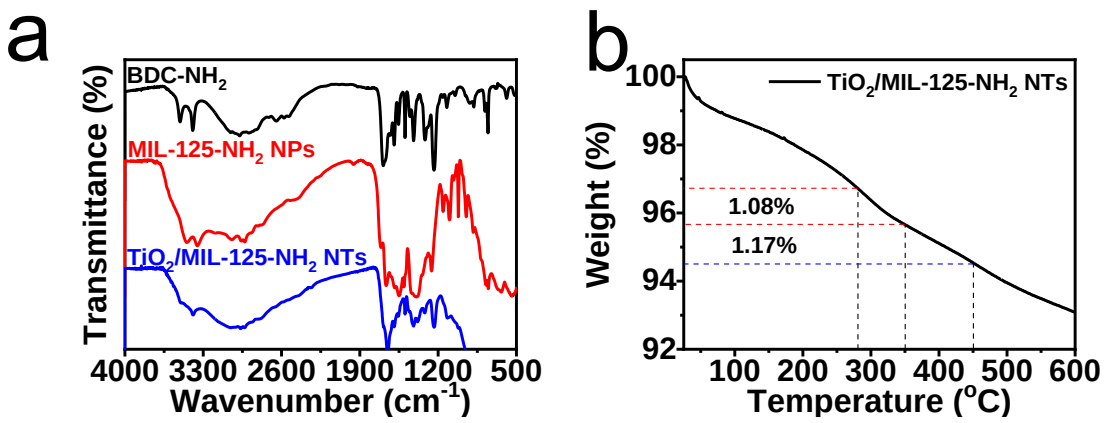

Figure S4. (a) FTIR spectra of TiO_2/MIL-125-NH_2 NTs, MIL-125-NH_2 NPs, and BDC-NH_2. (b) TGA curve of TiO_2/MIL-125-NH_2 NTs (heating rate of 10 ℃/min).

To determine the load of MIL-125-NH_2 on the resulted sample, TiO_2/MIL-125-NH_2 NTs was investigated by thermogravimetric analysis (TGA). The first weight loss from 25 to 100 ^oC is attributed to methanol, which is used as a washing solvent (1.21 %). The weight loss from 100 to 280 ^oC can be attributed to the departure of DMF and the free guest molecules which are not combined (2.04 %). Considering MIL-125 decompose (weight loss 1.17%) in the temperature range from 350 to 450 ^oC,[S1] the weight loss (1.08 %) in the temperature range from 280 to 350 ^oC can be attributed to the decomposition of MIL-125-NH_2. This result suggests that ~50% MIL-125 was transferred to MIL-125-NH2 via the ligands exchange technique.

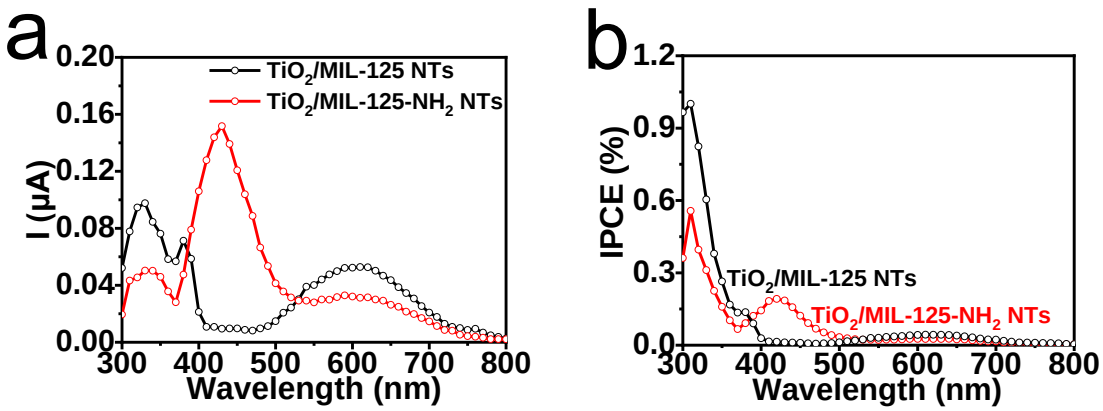

Figure S5. (a) Photocurrent spectra and (b) the corresponding IPCE of TiO_2/MIL-125 NTs and TiO_2/MIL-125-NH_2 NTs. The photocurrent spectra were measured using a xenon lamp (500 W) equipped with a monochromator. All tests were performed at room temperature in a 0.1 M Na_2SO_4 at a bias potential of 0.5 V in the wavelength range of 300-800 nm (with 10 nm steps).

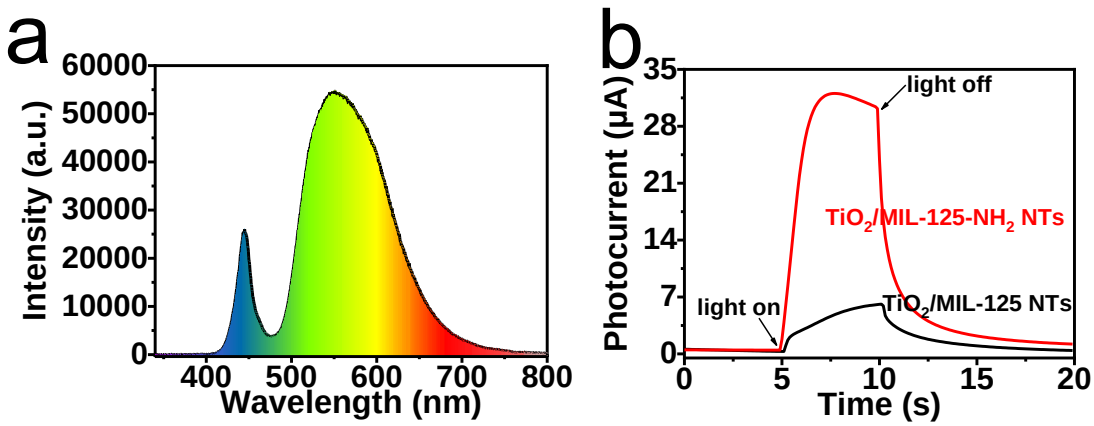

Figure S6. (a) Emission spectra of LED light used in this study. (b) Comparison of photocurrent response of TiO_2/MIL-125 NTs and TiO_2/MIL-125-NH_2 NTs based electrodes under LED-light irradiation (50 mW/cm^2). The PEC measurements were performed in 0.1 M Na_2SO_4 at a bias of +0.5 V.

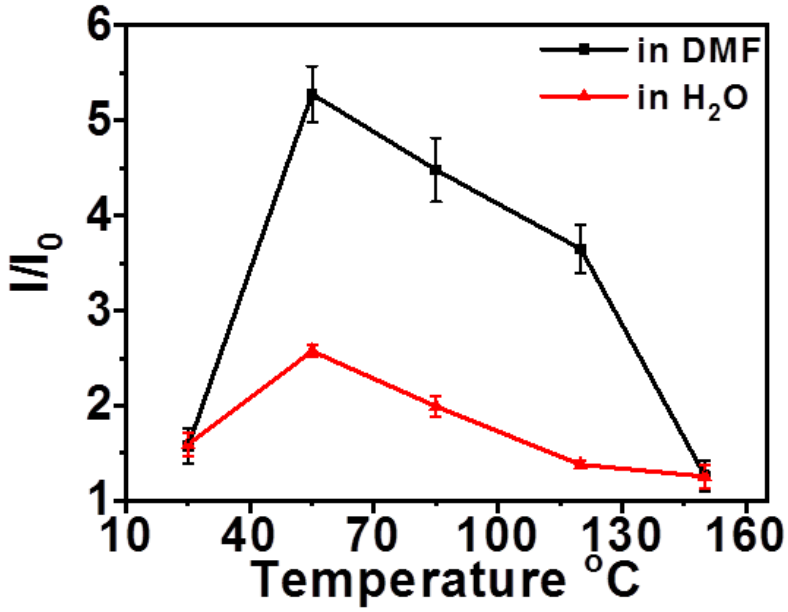

Figure S7. Photocurrent response of TiO_2/MIL-125 NTs based PEC electrodes after undergoing ligand-exchange reaction for 12 h in DMF or H_2O electrolyte containing 2.5 mM BDC-NH_2 at different temperatures.

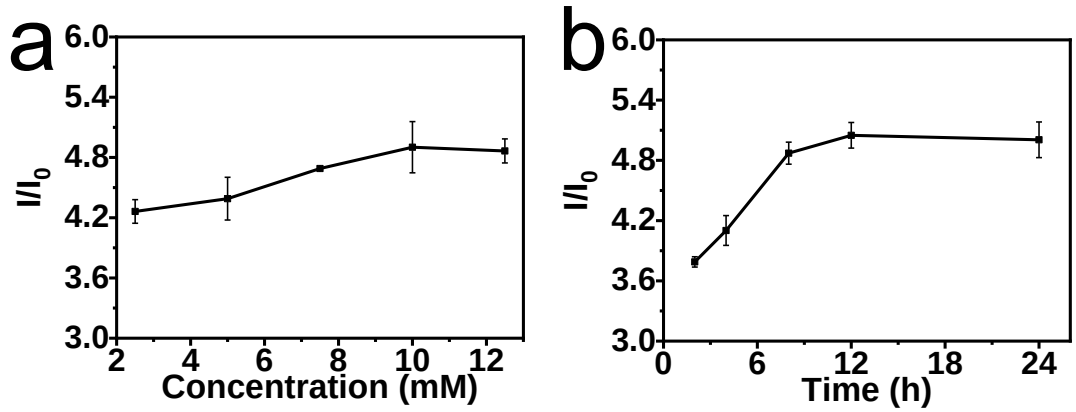

Figure S8. (a) Photocurrent response of TiO_2/MIL-125 NTs based PEC electrodes after undergoing ligand-exchange reaction for 12 h at 55 °C in DMF electrolyte containing different concentrations of BDC-NH_2. (b) Photocurrent response of TiO_2/MIL-125 NTs based PEC electrodes after undergoing ligand-exchange reaction at 55 °C in DMF electrolyte containing 10.0 mM BDC-NH_2 for different time periods.

Table S1. Atomic concentration table of TiO_2/MIL-125 NTs, TiO_2/MIL-125-NH_2 NTs, and TiO_2/MIL-125-NH-L-His NTs from XPS analysis.

Sample name	C 1s	N 1s	O 1s	Ti 2p
TiO_2/MIL-125 NTs (annealed)	19.38	1.52	56.70	22.40
TiO_2/MIL-125-NH_2 NTs	22.73	2.52	55.66	19.09
TiO_2/MIL-125-NH-L-His NTs	20.47	4.55	54.49	20.49

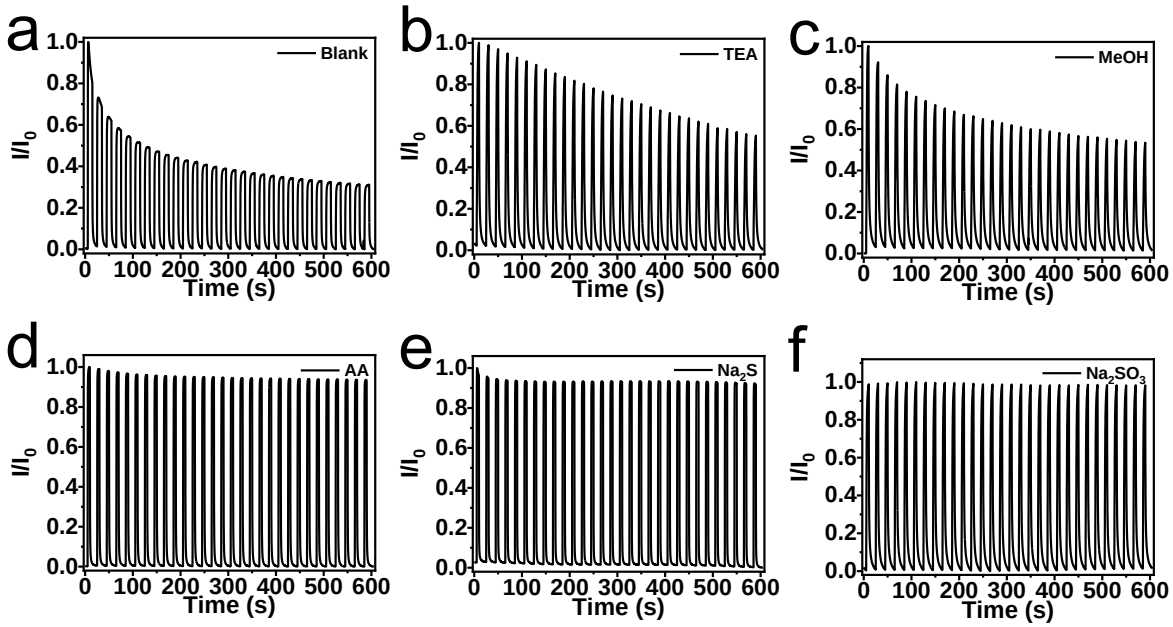

Figure S9. Stability of TiO_2/MIL-125-NH-L-His NTs electrode in 0.1 M Na_2SO_4 containing different sacrificial reagents: (a) blank, (b) 0.1 M TEA, (c) 20 vol% MeOH, (d) 0.1 M AA, (e) 0.1 M Na_2S, and (f) 0.1 M Na_2SO_3.

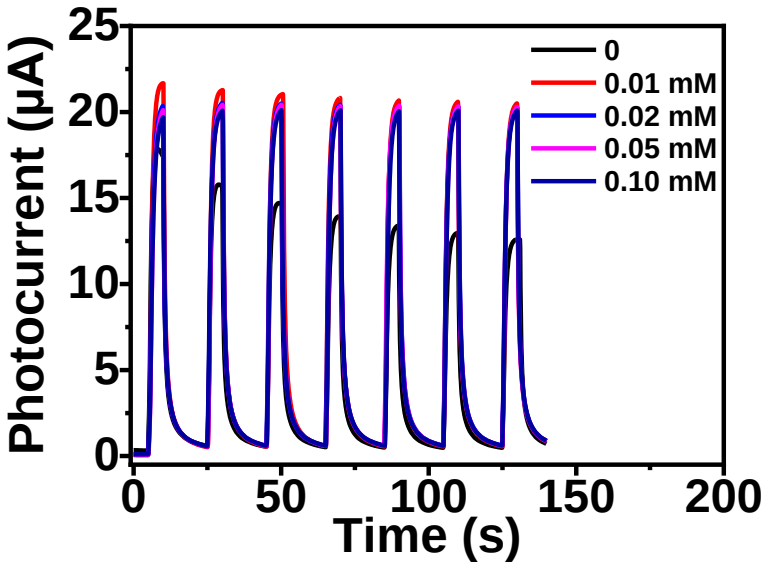

Figure S10. Photocurrent-time curves of TiO_2/MIL-125-NH-L-His NTs in 0.1 M Na_2SO_4 containing different concentrations of Na_2SO_3.

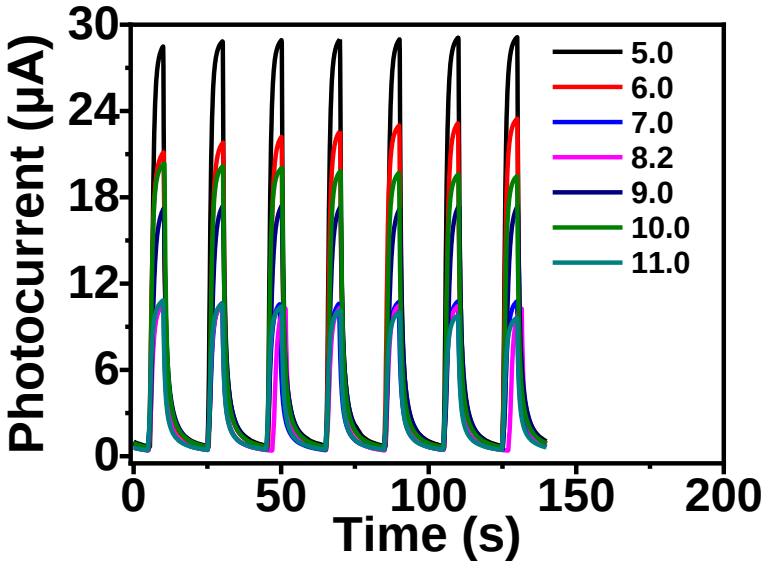

Figure S11. Photocurrent-time curves of TiO_2/MIL-125-NH-L-His NTs in 0.1 M Na_2SO_4 containing 0.05 M Na_2SO_3 of different pH values.

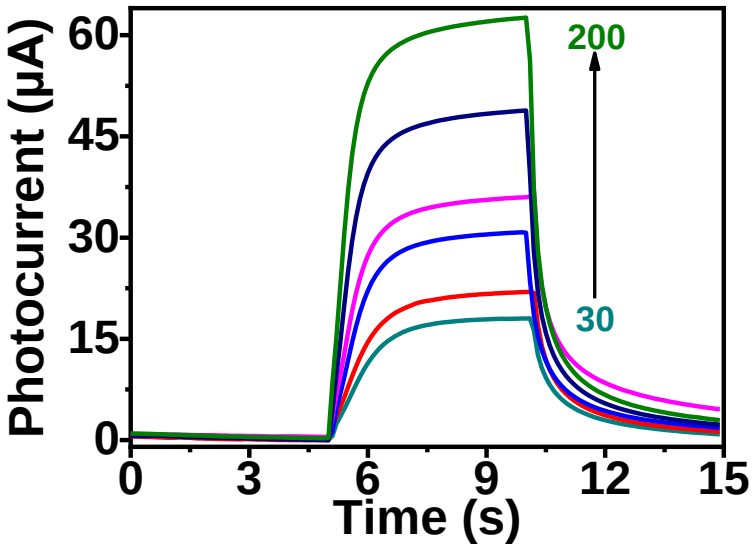

Figure S12. Photocurrent-time curves of TiO_2/MIL-125-NH-L-His NTs under different LED-irradiating intensities in 0.1 M Na_2SO_4 containing 0.05 M Na_2SO_3.

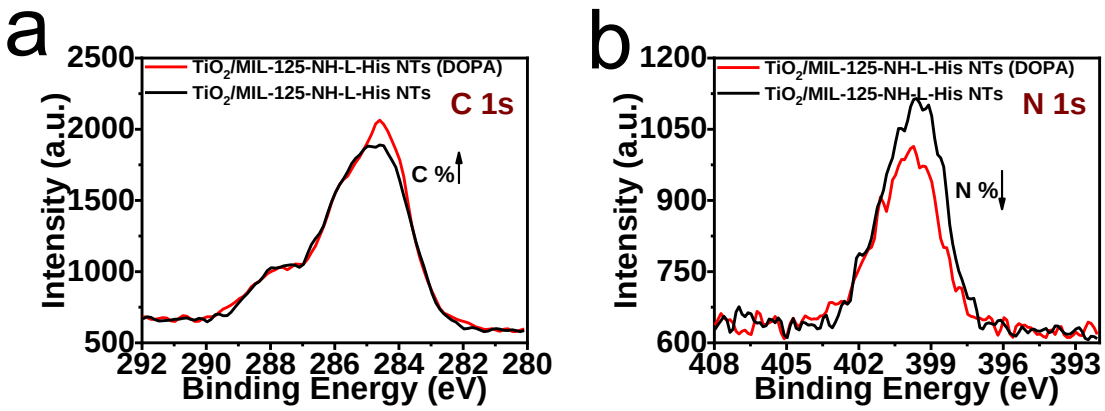

Figure S13. Core-level XPS peaks: (a) C 1s and (b) N 1s signals of TiO_2/MIL-125-NH-L-His NTs before and after L-DOPA recognition.

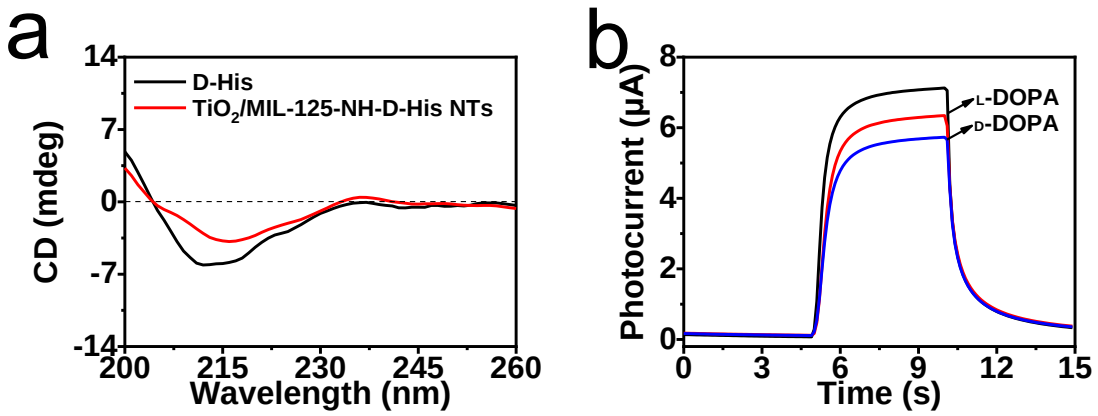

Figure S14. (a) CD spectra of D-His and TiO_2/MIL-125-NH-D-His NTs, (b) photocurrent of TiO_2/MIL-125-NH-D-His NTs before and after incubating in 20 μM L-/D-DOPA for 60 min.

Table S2. Comparison of various methods for L/D-DOPA detection.

Material	Method	Sensitivity data	Reference
Chirally imprinted mesoporous platinum	Differential pulse Voltammetry (DPV)	4 mM	S2
L-cysteine-gold nanoparticles	Colorimetric assay	1 μM	S3
Chiral poly(3,4-ethylenedioxythiophene) (PEDOT) derivatives	Electrochemical sensing	250 μM	S4
Cyclodextrin anchored grapheme nanohybrids	Electrochemical method	14.9 μM	S5
Enantioselective nanozyme AuNPs	Colorimetric strategy	100 μM	S6
Chiral (6,5) single-walled carbon nanotubes (SWCNTs)	DPV method	25 μM	S7
Gold nanodendrite (AuND) membrane	Electrochemical sensing	2.5 μM	S8
TiO_2/MIL-125-NH-L-His NTs PEC platform	PEC sensing	0.24 μM	This work

Reference

[S1] Dan-Hardi, M.; Serre, C.; Frot, T.; Rozes, L.; Maurin, G.; Sanchez, C.; Ferey, G. A New Photoactive Crystalline Highly Porous Titanium(IV) Dicarboxylate. *J. Am. Chem. Soc.* **2009**, *131*, 10857–10859.

[S2] Wattanakit, C.; Saint Come, Y. B.; Lapeyre, V.; Bopp, P. A.; Heim, M.; Yadnum, S.; Nokbin, S.; Warakulwit, C.; Limtrakul, J.; Kuhn, A. Enantioselective Recognition at Mesoporous Chiral Metal Surfaces. *Nat. Commun.* **2014**, *5*, 3325.

[S3] Zhang, L.; Xu, C. L.; Song, G. X.; Li, B. X. Self-Assembly of L-Cysteine-Gold Nanoparticles as Chiral Probes for Visual Recognition of 3,4-Dihydroxyphenylalanine Enantiomers. *RSC Adv.* **2015**, *5*, 27003.

[S4] Dong, L. Q.; Zhang, L.; Duan, X. M.; Mo, D. Z.; Xu, J. K.; Zhu, X. F. Synthesis and Characterization of Chiral PEDOT Enantiomers Bearing Chiral Moieties in Side Chains: Chiral Recognition and Its Mechanism Using Electrochemical Sensing Technology. *RSC Adv.* **2016**, *6*, 11536−11545.

[S5] Ates, S.; Zor, E.; Akin, I.; Bingol, H.; Alpaydin, S.; Akgemci, E. G. Discriminative Sensing of DOPA Enantiomers by Cyclodextrin Anchored Graphene Nanohybrids. *Anal. Chim., Acta* **2017**, *970*, 30−37.

[S6] Zhou, Y.; Sun, H. J.; Xu, H. C.; Matysiak, S.; Ren, J. S.; Qu, X. G. Mesoporous Encapsulated Chiral Nanogold for Use in Enantioselective Reactions. *Angew. Chem. Int. Ed.* **2018**, *57*, 16791−16795.

[S7] Pu, C. L.; Xu, Y. X.; Liu, Q.; Zhu, A. W.; Shi, G. Y. Enantiomers of Single Chirality Nanotube as Chiral Recognition Interface for Enhanced Electrochemical Chiral Analysis. *Anal. Chem.* **2019**, *91*, 3015−3020.

[S8] Lian, H. T.; Huang, S. Z.; Wei, X. F.; Guo, J. L.; Sun, X. Y.; Liu, B. Gold Nanodendrite-Based Differential Potential Ratiometric Sensing Strategy for Enantioselective Recognition of DOPA. *TALANTA* **2020**, *210*, 120654.